Electronic Supplementary Material (ESI) for Journal of Materials Chemistry C.

Supporting Information

An Angularly Fused Bistetracene: Facile Synthesis, Crystal Packing and Single-Crystal Field Effect Transistors

Zunzhi Wang,† Rongjin Li,† Yulan Chen,† Yuan-Zhi Tan,ς Zeyi Tu,‡ Xuejiao J. Gao,¶ Huanli Dong,‡ Yuanping Yi,‡ Yu Zhang,† Wenping Hu,*,†,‡ Klaus Müllen,*,§ and Long Chen*,†

†Department of Chemistry and Tianjin Key Laboratory of Molecular Optoelectronic Science, Tianjin University, Tianjin 300072, China

‡Institute of Chemistry, Chinese Academy of Science, Beijing 100190, China

ςDepartment of Chemistry, College of Chemistry and Chemical Engineering, Xiamen University, Xiamen 361005, China

¶Institute of High Energy Physics, Chinese Academy of Science, Beijing 100049, China

§Max Planck Institute for Polymer Research, Ackermannweg 10, 55128 Mainz, Germany

**E-mail: hwp@iccas.ac.cn; muellen@mpip-mainz.mpg.de; long.chen@tju.edu.cn*

Section 1. Materials and Methods

All starting materials were directly used from commercial sources without further purification. THF was dried over sodium benzophenone prior to distillation under nitrogen. ^{1}H NMR and ^{13}C NMR spectra were recorded in deuterated solvents on a Bruker ADVANCE 400 operating at 400 MHz (^{1}H NMR) and 100 MHz (^{13}C NMR) or Bruker ADVANCE 500 operating at 500 MHz (^{1}H NMR) and 125 MHz (^{13}C NMR). Signals were referenced to residual solvent peaks (δ in parts per million (ppm) ^{1}H: $CDCl_3$, 7.26 ppm, $C_2D_2Cl_4$, 6.0 ppm, DMSO-d_6, 2.50 ppm, C_6D_6, 7.16 ppm; ^{13}C: $CDCl_3$, 77.23 ppm, $C_2D_2Cl_4$, 73.78 ppm, DMSO-d_6, 39.51 ppm, C_6D_6, 128.39 ppm). Coupling constants were assigned as observed. MALDI-TOF mass spectra were recorded on a Bruker New Autoflex Speed LIN Spectrometer using a 337 nm nitrogen laser with dithranol as matrix. High resolution mass spectra were recorded from Bruker micro TOF II (ESI) instrument. UV/Vis spectra were recorded on a SHIMADZU UV-3600 spectrometer. Fluorescence spectra were recorded at 25 °C on a Hitachi model F-7000 spectrofluorometer and corrected for wavelength-dependent detector sensitivity and excitation light source output. The absolute fluorescence quantum yields were recorded by Steady-Transient Fluorescence Spectrometer model FLS920 produced by EDINBURGH. Quantum yields were determined according to published procedures,[S1] calculated by the following equation: $\Phi_x = \Phi_{st}\ (1\text{-}R_{st}I_x)/(1\text{-}R_xI_{st})$. R_x and R_{st} represent diffuse reflectance of the sample and the standard, respectively (in a particular wavelength). $\Phi_x = \Phi_{st}$ are the quantum yields of liquid samples and the standard, respectively. I_x and I_{st} represent the integrated emission spectrum of the sample and the standard, respectively. Cyclic voltammetry (CV) studies were performed in 0.1 M $TBAPF_6$ in THF solutions with a scan rate of 50 mV/s on a CHI 660 electrochemical workstation using glassy carbon discs as the working electrode, Pt wire as the counter electrode, Ag/AgCl electrode as the reference electrode, and ferrocene/ferrocenium as an internal potential marker for the calibration of potential. The HOMO, LUMO energy levels for BT-nTIPS (n = 2, 3, 4) were estimated on the basis of an oxidation potential of -4.8 eV (below vacuum level) for Fc/Fc^+. Compound **1** was synthesized according to the literature.[S2] All reported yields are isolated yields.

To compute the HOMOs and LUMOs of BT-2TPIS, BT-3TIPS, and BT-4TIPS, we firstly optimized their geometries using the B3LYP[S3] method in conjugation with the 6-31G(d, p) basis set for all atoms. Then, frequency analyses were done at the same level of theory, which confirmed that all optimized structures were energy minima without imaginary frequencies. The HOMOs and LUMOs were plotted using the Gaussview code based on the converged wave functions of the optimized structures. All geometry optimization and frequency analyses were done using the GAUSSIAN 09 package. [S4] For the calculation of transfer integrals and reorganization energies, the molecular geometries of the neutral, radical-cation, radical-anion states were optimized by density functional theory (DFT). The reorganization energies were calculated from the relevant points on the potential energy surface. The transfer integrals for molecular pairs taken from the experimental crystal structures were evaluated by using a fragment orbital approach[S5] in combination with a basis set orthogonalization procedure.[S6] These calculations were performed at the 6-31G**/B3LYP level of theory with the *Gaussian 09* package.[S4]

OFET device fabrication: A solution (around 0.5 mM) of BT-2TIPS, BT-3TIPS or BT-4TIPS (around 100 μL) in chlorobenzene was dropped on the OTS treated Si/SiO_2 substrates. Micro-ribbons were formed on the substrates after solvent evaporation in air under room temperature. Two methods were used to construct the FET devices:

(1) The "organic ribbon as shadow mask" method was used for the fabrication of single ribbon based OFET devices of BT-2TIPS and BT-3TIPS[S7]. Firstly, an individual ribbon standing on the SiO_2 surface, as an "organic ribbon mask", was selected and picked up by the van der Waals force using a mechanical probe and crossed over the target ribbon; this was performed on a Micromanipulator 6150 probe station with a high-resolution microscope (magnification at 400–1000 times). Then, gold source and drain electrodes (40 nm) were vacuum deposited on the crossed-ribbon structure; finally, the ''organic ribbon mask'' was peeled off, again using the mechanical probe. (2) The "gold layer glue" technique was used for the fabrication of single ribbon based OFET devices of BT-4TIPS [S8]. Firstly, Au thin film with a thickness of about 100 nm was pre-deposited on a Si wafer by thermal evaporation. Then, a piece of the Au film of around 50 by 500 μm^2 was scooped off the Si substrate with the tip of the mechanical probe and transferred onto the sub-micrometer-sized ribbons as a source or drain electrode. The current-voltage (I–V) characteristics of OFETs were recorded with a Keithley 4200 SCS and a Micromanipulator 6150 probe station in a clean and metallic shielded box at room temperature in air. **Device structure**: The devices adopt the "top-contact bottom-gate" geometry. The top source and drain electrodes were gold thin film with a thickness of around 100 nm prepared either by thermal evaporation or by the "gold layer glue" technique. The dielectric layer was thermally grown SiO_2 with a thickness of 300 nm modified by octadecyltrichlorosilane

(OTS). The gate was heavily doped Si. The diameters of the crystals forming the channel of the OFET were typically 1-3 μm.

Section 2. Synthesis

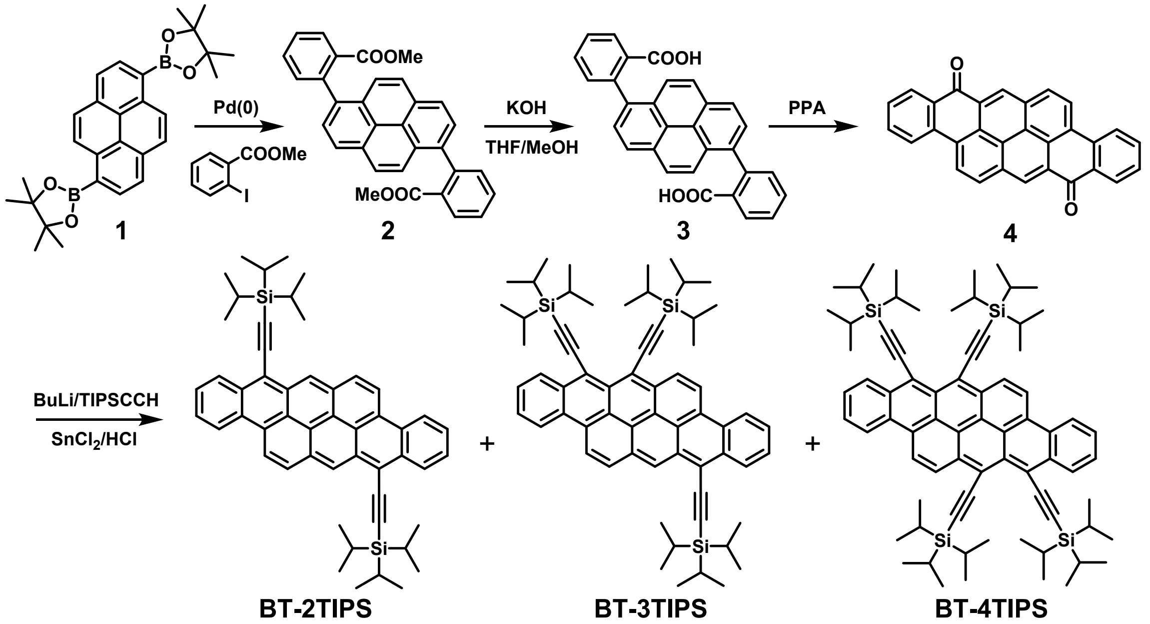

Scheme S1. Synthesis of **BT-2TPIS**, **BT-3TIPS**, and **BT-4TIPS**.

Compound 2

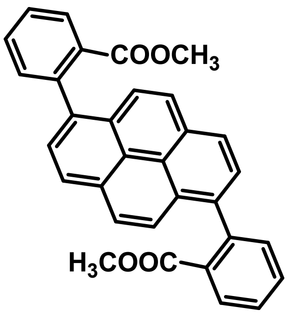

To a Schlenk flask was added compound **1** (1.81 g, 3.98 mmol), methyl 2-iodobenzoate (2.57 g, 9.81 mmol), tetrakis(triphenylphosphine)-palladium(0) (536 mg, 0.46 mmol), dried THF (200 mL), and 2 M potassium carbonate solution (76 mL) under N_2 atmosphere. The mixture was heated at 80 °C overnight with vigorous stirring. After cooled to room temperature, the organic phase was separated and washed twice with water, dried over sodium sulfate and concentrated in vacuum. The residue was purified by silica chromatographic column (eluent: EtOAc/Petroleum ether = 1/4 v/v) to afford a yellow solid **2** (0.93 g) with a yield of 49%. ^{1}H NMR (500 MHz, $C_2D_2Cl_4$) δ 8.21(d, J = 7.5 Hz, 2H), 8.15 (d, J = 7.0 Hz, 2H), 8.04 (d, J = 9.0 Hz, 2H), 7.92 (d, J = 7.5 Hz, 2H), 7.82 (d, J = 9.0 Hz, 2H), 7.74-7.68 (m, 2H), 7.63 (t, J = 7.0 Hz, 2H), 7.57 (dd, J = 11.5, 7.0 Hz, 2H), 3.40 (s, 6H). ^{13}C NMR ($C_2D_4Cl_2$, 125 MHz): 167.46, 141.71, 137.10, 132.25, 131.87, 131.15, 131.08, 130.24, 129.91, 129.04, 127.35, 127.26, 126.95, 124.82, 123.95, 51.37; HRMS (ESI): m/z calcd. for $C_{32}H_{22}O_4Na$ $[M+Na]^+$ 493.1416, found: 493.1419.

Compound 3

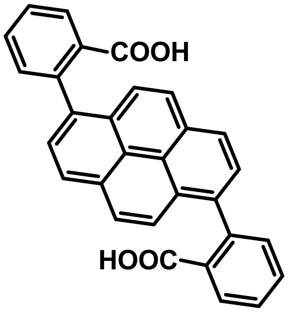

A mixture of compound **2**(517 mg, 1.09 mmol), KOH (0.92 g, 16.43 mmol), THF (15 ml) and methanol (5 ml) was heated at 90 °C for 12 h. After the removal of the solvent, HCl (36 %) was added to the filtrate until completely acidified. The formed precipitate was collected by filtration, washed with water, and then dried in oven to afford the product **3** (416 mg, 86%) as a yellow solid. ^{1}H NMR (400 MHz, DMSO-d_6) δ 12.40 (brs, 2H), 8.27 (dd, J = 8.0, 2.4 Hz, 2H), 8.12 (d, J = 9.2 Hz, 2H), 8.05 – 8.02 (m, 2H), 7.90-7.87 (m, 2H), 7.77-7.74 (m, 2H), 7.70 – 7.63 (m, 4H), 7.54-7.49 (m, 2H). ^{13}C NMR (100 MHz, DMSO-d_6): 168.29, 140.58, 137.47, 132.79, 131.90, 131.36, 129.78, 129.68, 128.39, 127.86, 127.40, 127.07, 124.44, 124.29, 123.89; HRMS (ESI): m/z calcd. for $C_{30}H_{18}O_4Na$ $[M+Na]^+$ 465.1103, found: 465.1110.

Compound 4

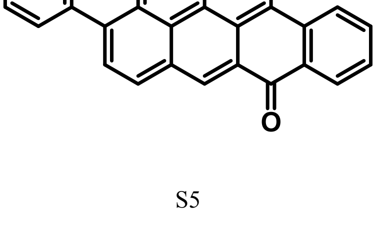

Compound **3** (104 mg, 0.24 mmol) was added to polyphosphoric acid (PPA, 5ml) at 90 °C under nitrogen atmosphere. The dark red mixture was further heated at 120 °C for 48 h. After cooling to room temperature, the mixture was poured into an ice-water mixture (300 mL) with $NaHCO_3$. The precipitate was filtered, washed with water (300 mL) and then methanol, and acetone, finally dried to give compound **4** as red black solid (90 mg, 95%). The product is not soluble for ^{1}H and ^{13}C NMR spectrum and was used directly for next step. HRMS (ESI): m/z calcd. for $C_{30}H_{15}O_2$ $[M+H]^+$ 407.1072, found: 407.1072.

Compound BT-2TIPS, **BT-3TIPS**, and **BT-4TIPS**

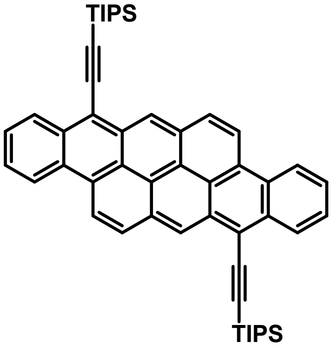

,

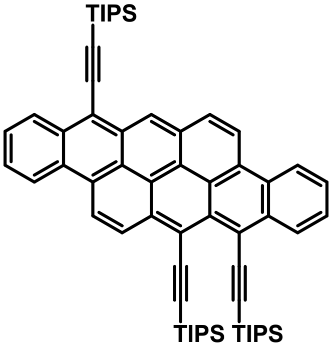

,

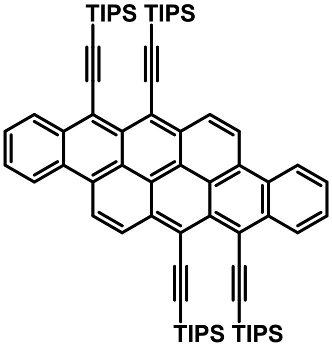

To a solution of triisopropylsilylacetylene (318 mg, 1.74 mmol) in dry THF (5 ml), of 2.5 M n-BuLi (0.75 mL) at 0 °C was added dropwise. The solution was allowed to stir at 0 °C for 1 h before the addition of **4** (71 mg, 0.17 mmol). The mixture was warmed to room temperature and stirred for 6 h. A solution of $SnCl_2.2H_2O$ (259 mg, 1.15 mmol) in 3 M HCl (0.65 mL) was added to the solution at room temperature, it was stirred for another 3 h and then poured into water (10 mL), extracted with DCM, and dried over $MgSO_4$. After the solvent was evaporated, the crude product (ca. 80 mg) was re-dissolved in THF (50 mL) and mixed with silica gel (ca. 10 g). The solvent was further evaporated to dryness, and the resulted crude product@silica was loaded on a short silica chromatographic column using petroleum ether as eluent to collect the first blue-green faction. The products were further separated by a GPC column (Bio-Beads S-X1 Support: 200-400 mesh) using THF as eluent to provide BT-2TIPS (32 mg, 26%) as a dark purple solid. Additionally, compound BT-3TIPS (19 mg, 12%) and BT-4TIPS (4 mg, 2%) was obtained as a lightly green solid and a green solid respectively.

Compound BT-2TIPS

^{1}H NMR (400 MHz, THF-d8) δ 9.62 (m, 2H), 9.38-9.28 (m, 2H), 9.23-9.18 (m, 2H), 9.05-8.93 (m, 2H), 8.53-8.42 (m, 2H), 7.95-7.82 (m, 4H), 1.62-1.37 (m, 42H). HRMS (ESI): m/z calcd. for $C_{52}H_{57}Si_2$ $[M+H]^+$ 737.3999, found: 737.3997. UV/Vis (THF): λ_{max} (nm) (ε / $M^{-1}cm^{-1}$) 354 (2.48×10^4), 648 (1.60×10^4).

Compound BT-3TIPS

^{1}H NMR (400 MHz, C_6D_6) δ 9.71 (s, 1H), 9.53 (d, *J* = 8.0 Hz, 2H), 9.22 (d, *J* = 8.4 Hz, 1H), 8.94 (d, *J* = 9.6 Hz, 1H), 8.66 (d, *J* = 8.8 Hz, 1H), 8.61 (d, *J* = 8.8 Hz, 1H), 8.57 (d, *J* = 9.6 Hz, 1H), 8.22 (d, *J* = 9.2 Hz, 1H), 7.72-7.69 (m, 1H), 7.63-7.59 (m, 1H), 7.50-7.45 (m, 2H), 1.48 – 1.43 (m, 63H). HRMS (ESI): m/z calcd. for $C_{63}H_{77}Si_3$ $[M+H]^+$ 917.5333, found: 917.5381. UV/Vis (THF): λ_{max} (nm) (ε / $M^{-1}cm^{-1}$) 361 (2.32×10^4), 693 (1.02×10^4).

Compound BT-4TIPS

^{1}H NMR (400 MHz, $CDCl_3$) δ 9.23 (d, J = 8.0 Hz, 2H), 9.16-9.12 (m, 4H), 9.08-9.06 (m, 2H), 7.87-7.85 (m, 4H), 1.25-1.23 (m, 84H). HRMS (ESI): m/z calcd. for $C_{74}H_{97}Si_4$ $[M+H]^+$ 1097.6667, found: 1097.6667. UV/Vis (THF): λ_{max} (nm) (ε / $M^{-1}cm^{-1}$) 366 (8.06×10^4), 728 (7.37×10^4).

Section 3. Photophysical Properties

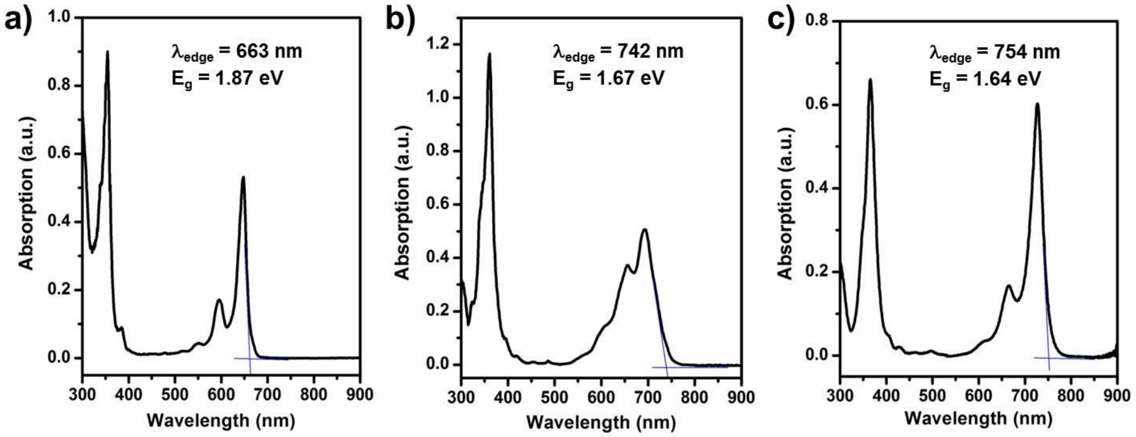

Figure S1. UV-vis absorption specta of a) BT-2TIPS in 2.5×10^{-6} M; b) BT-3TIPS in 5×10^{-6} M; c) BT-4TIPS in 5×10^{-6} M THF solution.

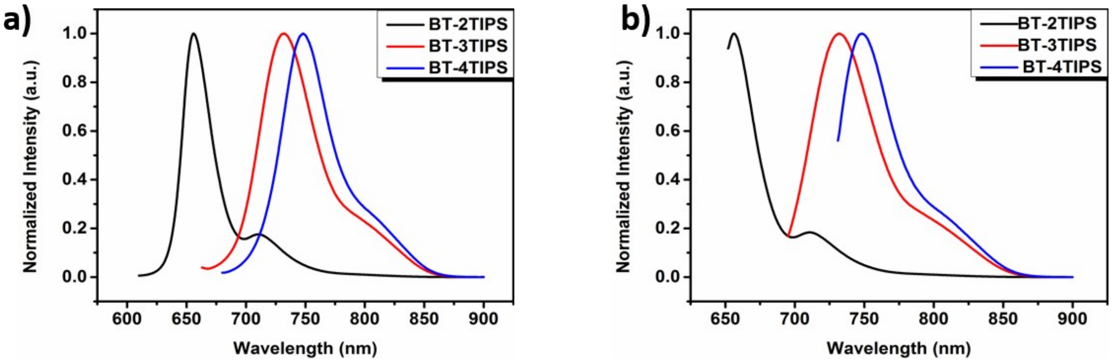

Figure S2. Normalized fluorescence spectra of BT-2,3,4TIPS which were excited at a) 598 nm, 657 nm, 667nm; b) 650 nm, 693 nm, 730 nm respectively in THF solution. The data were obtained on a Shimadzu F-7000 at room temperature.

Section 4. UV-vis Spectroscopic Stability Studies

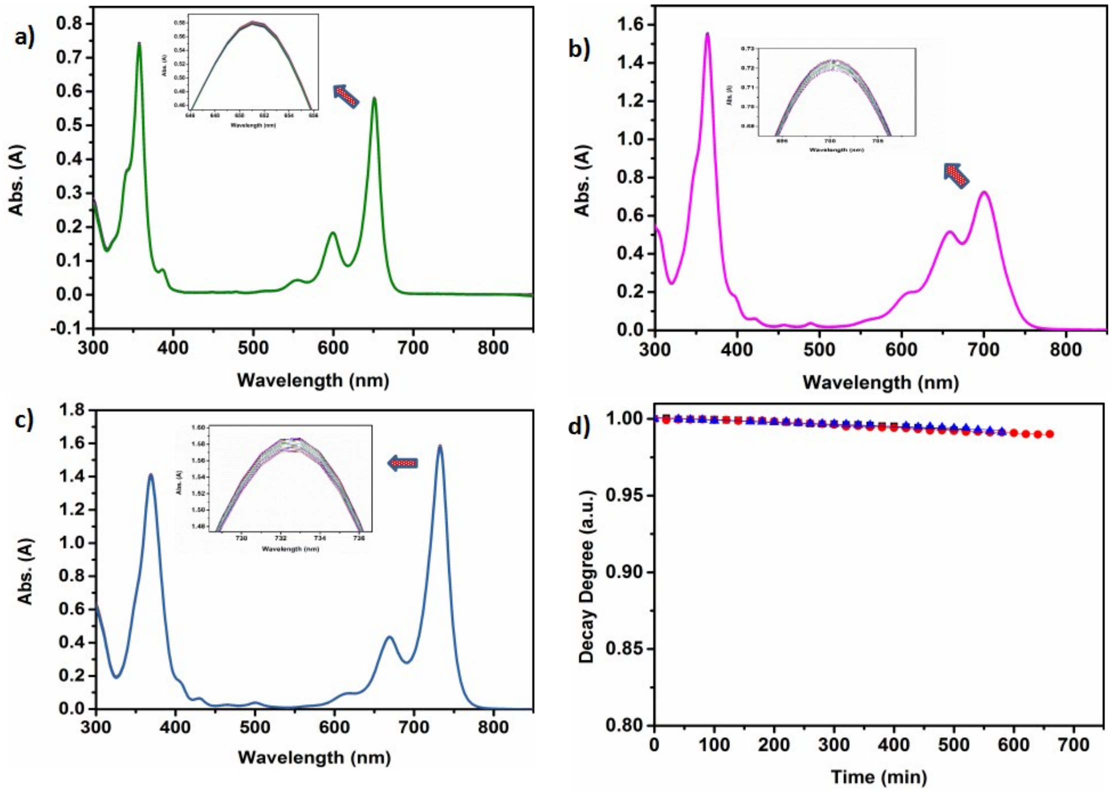

Figure S3. The monitored UV-vis absorption of a) BT-2TIPS (inset: gradual decrease of the absorption signal at 651 nm); b) BT-3TIPS (inset: gradual decrease of the absorption signal at 700 nm) and c) BT-4TIPS (inset: gradual decrease of the absorption signal at 733 nm) overtime in toluene without light over 2 days. d) Degree of degradation of BT-2TIPS (blue), BT-3TIPS (black) and BT-4TIPS (red) *vs* time in toluene in the absence of light. These compounds displayed scarcely decomposition under exclusion of light even in the presence of oxygen.

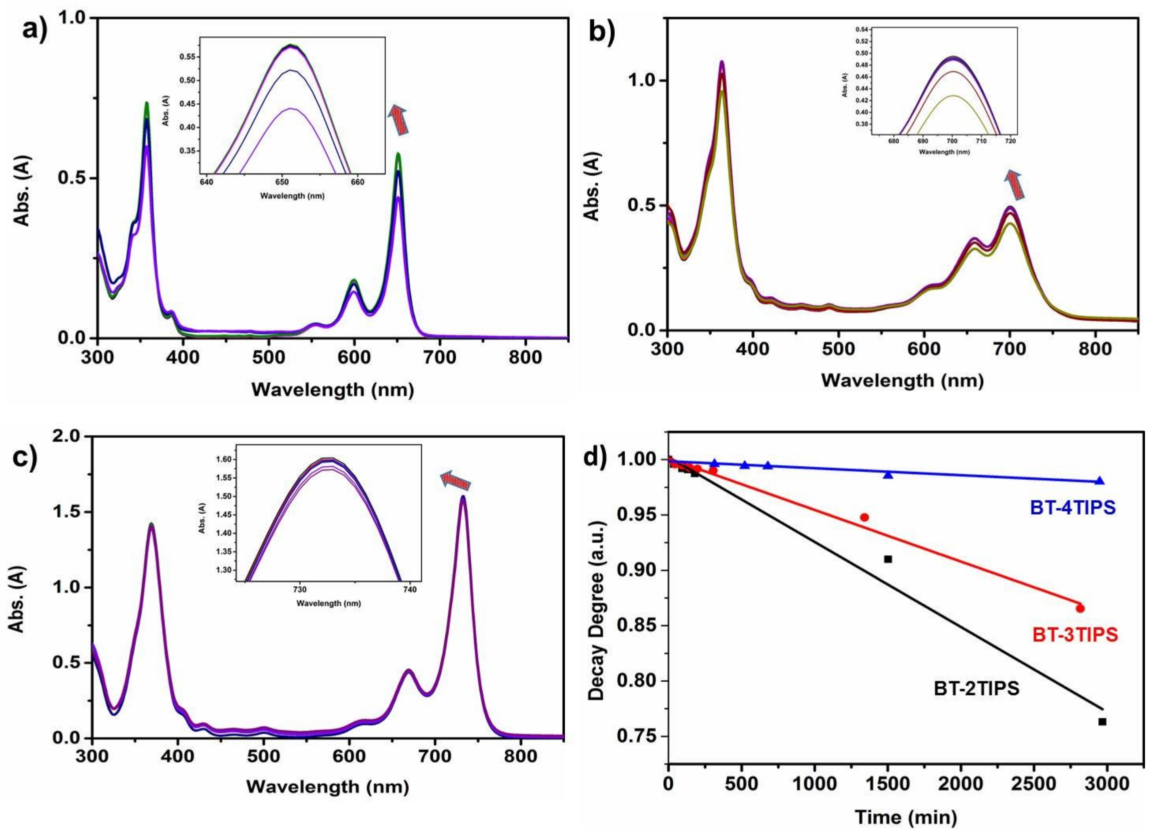

Figure S4. The monitored UV-vis absorption of a) BT-2TIPS (inset: gradual decrease of the absorption signal at 651 nm); b) BT-3TIPS (inset: gradual decrease of the absorption signal at 700 nm) and c) BT-4TIPS (inset: gradual decrease of the absorption signal at 733 nm) overtime in toluene upon ambient light and air. d) Degree of degradation of BT-2TIPS (black, $y=1.00235-7.67719*10^{-5}x$, $R^2=0.98201$, half-time: 4.54 days); BT-3TIPS (red, $y=1.00108-4.65807*10^{-5}x$, $R^2=0.98989$, half-time: 7.47 days); BT-4TIPS (blue, $y=0.99826-6.61449*10^{-6}x$, $R^2=0.93872$, half-time: 54.88 days) *vs* time in toluene upon ambient light and air.

Table S1. Decay of BT-2TIPS, BT-3TIPS, and BT-4TIPS at maximum absorption in toluene upon ambient light and air vs time.

Time (min)	**Degree of Degradation (BT-2TIPS)**	**Time (min)**	**Degree of Degradation (BT-3TIPS)**	**Time (min)**	**Degree of Degradation (BT-4TIPS)**
0	1	0	1	0	1
36	0.99586	96	0.99475	315	0.99607
93	0.99191	146	0.99270	522	0.99432
133	0.99098	198	0.99157	679	0.99392
181	0.98740	306	0.99002	1053	0.98554
1502	0.91000	1341	0.94773	2948	0.98024
2968	0.76314	2817	0.86539		

Section 5. Cyclic Voltammetry and Energy Levels

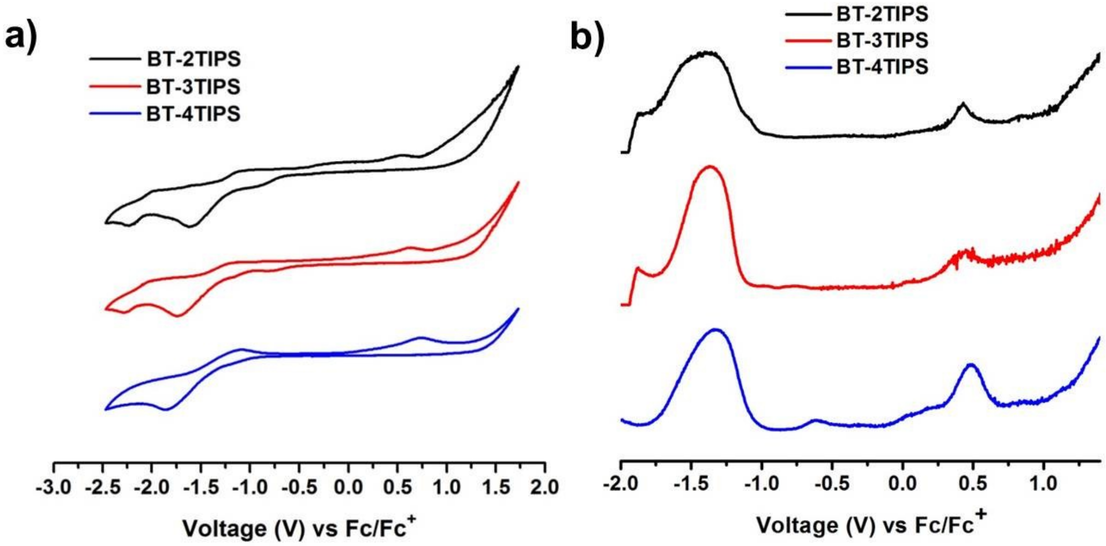

Figure S5. a) Cyclic voltammograms of BT-2TIPS, BT-3TIPS, and BT-4TIPS in THF (0.5 mM; BT-2TIPS in black, BT-3TIPS in red, and BT-4TIPS in blue); b) Differential pulse voltammograms of BT-2TIPS, BT-3TIPS, and BT-4TIPS in THF (0.5 mM; BT-2TIPS in black, BT-3TIPS in red, and BT-4TIPS in blue)

Table S1. Optical and electronic properties of BTs.

Compound	**λ_{abs} (nm)**	**λ_{onset} (nm)[a]**	**E_{ox1} (V)[b]**	**LUMO (eV)[c]**	**HOMO (eV)[d]**	**E_G^{cal} (eV)[e]**	**E_G^{opt} (eV)[f]**
BT-2TIPS	648	663	0.25	-3.18	-5.05	1.79	1.87
BT-3TIPS	693	742	0.20	-3.33	-5.00	1.65	1.67
BT-4TIPS	728	754	0.21	-3.37	-5.01	1.51	1.64

[a]Onset wavelengths (λ_{onset}) were determined by constructing a tangent at the point of inflection of the bathochromic slop of the most red-shifted; [b]Onset potentials, determined by cyclic voltammetric measurements in 0.1 M solution of Bu_4NPF_6 in THF vs Fc^+/Fc; [c]Estimated vs vacuum level from $E_{LUMO} = -4.80$ eV $- E_{red1}$; [d]$E_{HOMO} = E_{LUMO} - E_G^{opt}$; [e]Calculated band gap $E_G^{opt} = E_{LUMO}^{cal} - E_{HOMO}^{cal}$; [f]Optical band gap $E_G^{opt} = 1240/\lambda_{onset}$.

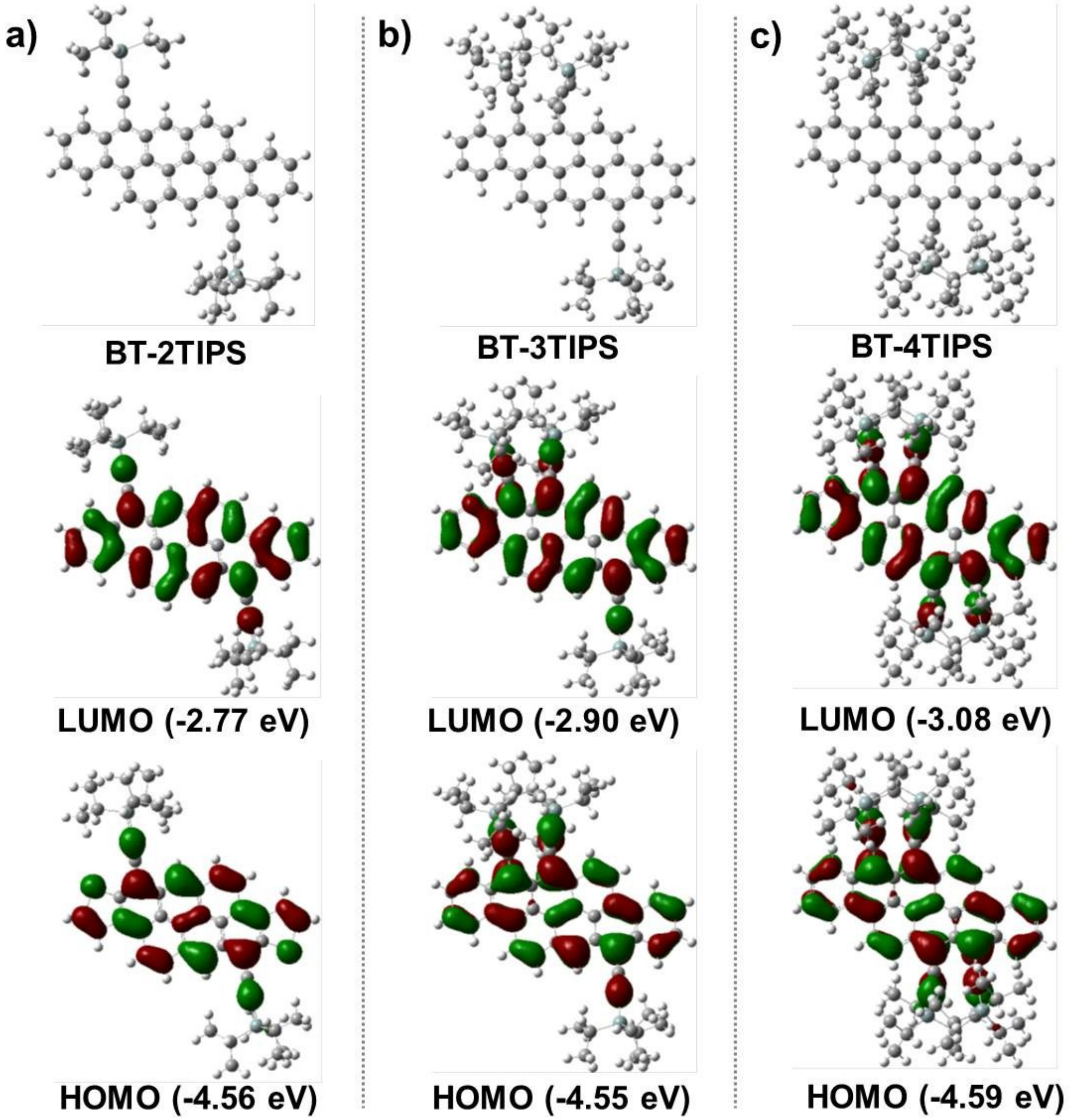

Figure S6. Frontier molecular orbitals of BT-2TIPS, BT-3TIPS, BT-4TIPS and their energy levels derived by means of B3LYP/6-31G(d, p) DFT calculations.

Section 6. X-ray Crystallographic Structure Determination and device images

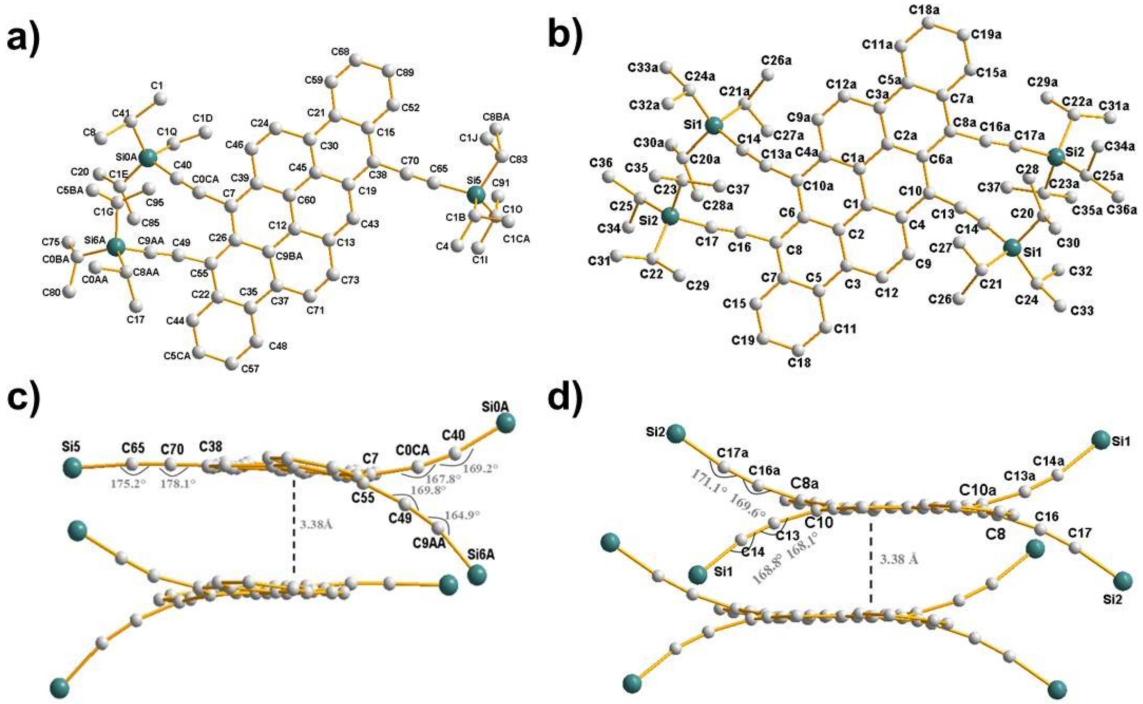

Figure S7. Molecular structure and atomic numbering of a) BT-3TIPS and b) BT-4TIPS in the solid state (ellipsoids are set 50 % probability; H atoms have omitted for clarity). Packing of c) BT-3TIPS and d) BT-4TIPS in the solid state highlighting the π-π stacked dimers (both interplanar distance are 3.38 Å) and the bending of the alkyne branches out of the molecular plane (H atoms and triisopropyl groups have been omitted for clarity).

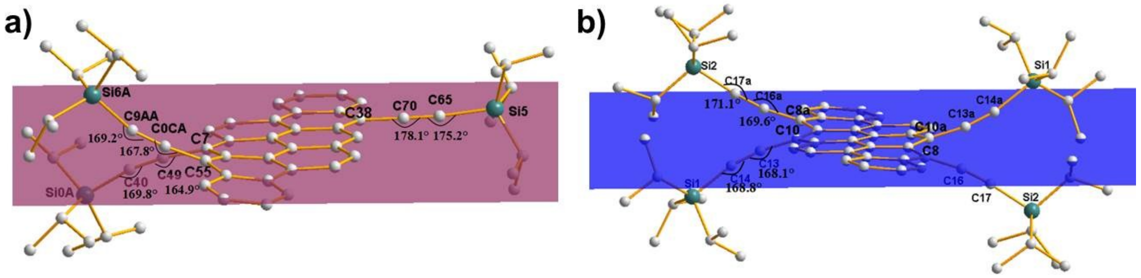

Figure S8. a) Calculated mean plane of the 30 core C-atoms of a) BT-3TIPS in violet and b) BT-4TIPS in blue. In the case of BT-3TIPS, all of the core C-atoms are essentially in-plane except for C55 which deviate from the plane by 0.22 Å; while in the case of BT-4TIPS, all the 28 core C-atoms are in-plane except for C10 and C8 which deviate from the plane by 0.19 and 0.15 Å, respectively.

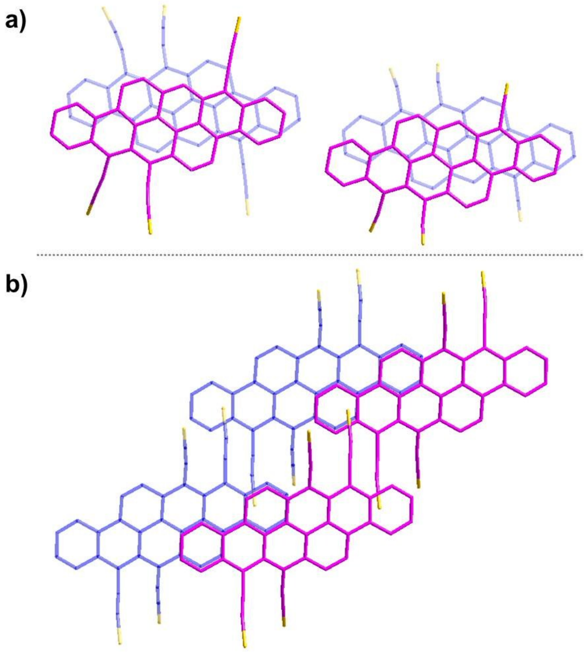

Figure S9. Crystal packing of a) BT-3TIPS and b) BT-4TIPS. Hydrogen atoms and triisopropyl groups were omitted for clarity. Good π-overlap is visible for each π-stacked dimer. The π-overlap between two face-to-face molecules in BT-3TIPS amounts to nearly five full benzene rings while in the case of BT-4TIPS is about two benzene rings.

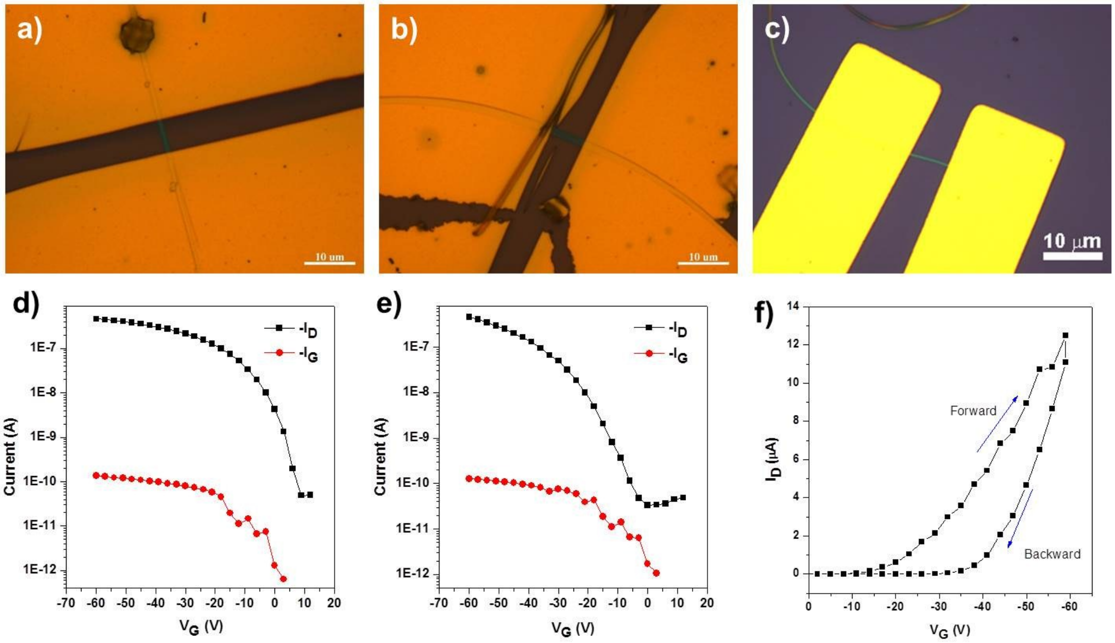

Figure S10. Representative microscopy images of the single crystal based devices a) BT-2TIP, b) BT-3TIPS, and c) BT-4TIPS with scale bar of 10 μm; the leakage currents (I_{GS}) for d) BT-2TIPS and e) BT-3TIPS; f) transfer characteristics of BT-2TIPS scanning gate voltage both forward and backward, showing notable hysteresis. The mobility changed little as calculated from the forward and backward scan (the mobility increased about 10%

in the backward scan). However, the threshold voltage increased drastically from -28 V to -42 V, which were tentatively ascribed to the trapping of water and/or oxygen during the measurements.

Section 7. Calculation of transfer integrals, reorganization energies and theoretical mobilities

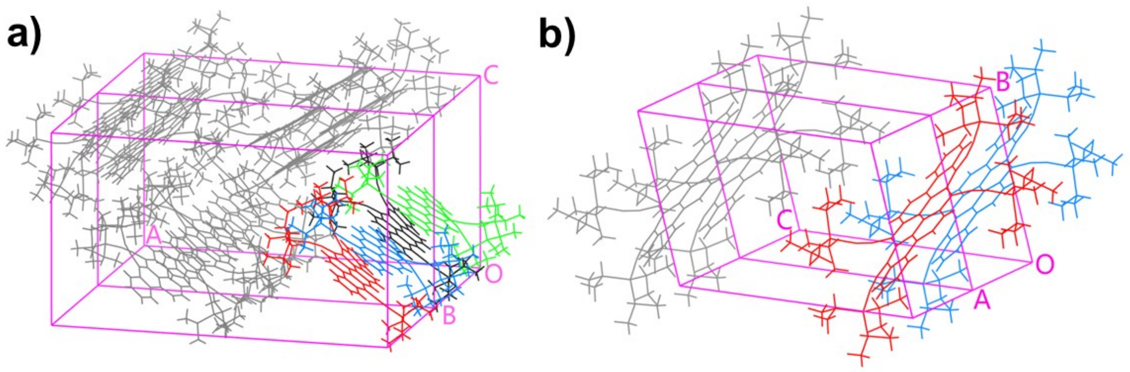

Figure S11. Illustration of molecular dimers for transfer integrals calculations in (a) BT-3TIPS and (b) BT-4TIPS crystals.

Table S2. Hole and electron transfer integrals (t_h and t_e, in meV) and centroid distances (d, in Å) for the molecular pairs taken from the corresponding crystals (r: red, b: blue, k: black, g: green).

system	dimer	d	t_h	t_e
BT-3TIPS	r,b (k,g)	4.78	53.8	41.2
	r,k	16.58	1.3	7.4
	b,g	16.58	1.2	6.5
	b,k	17.43	0.1	0.3
BT-4TIPS	π-π	7.49	44.3	62.9

Table S3. Intramolecular reorganization energies (in meV) for holes (λ_h) and electrons (λ_e).

	λ_h^+	λ_h^0	λ_h	λ_e^-	λ_e^0	λ_e
BT-2TIPS	65	65	130	90	89	179
BT-3TIPS	70	71	141	96	94	190
BT-4TIPS	72	72	144	92	91	183

$\lambda^{\pm}$ represents the relaxation energy in the cationic/anionic state in going from the neutral to the ionic geometry, and λ^0 the relaxation energy in the ground state in going from the ionic to the neutral geometry.

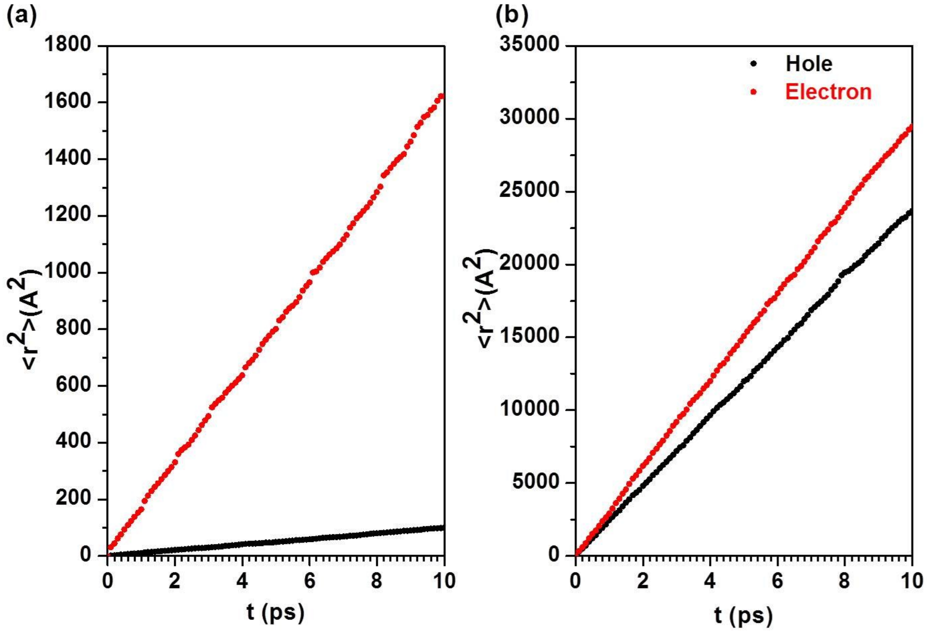

Figure S12. Mean squared displacement of 5000 independent trajectories versus simulation time at 300 K: a) BT-3TIPS, b) BT-4TIPS.

The hole/electron mobilities using the transfer integrals and reorganization energies by means of kinetic Monte-Carlo simulations in combination with the Marcus charge-transfer theory based on the available crystal structures.[S9-10] The results are listed as follow:

	hole mobility (cm^2/Vs)	**electron mobility (cm^2/Vs)**
BT-3TIPS	1.90×10^{-3}	3.11×10^{-2}
BT-4TIPS	4.62×10^{-1}	5.73×10^{-1}

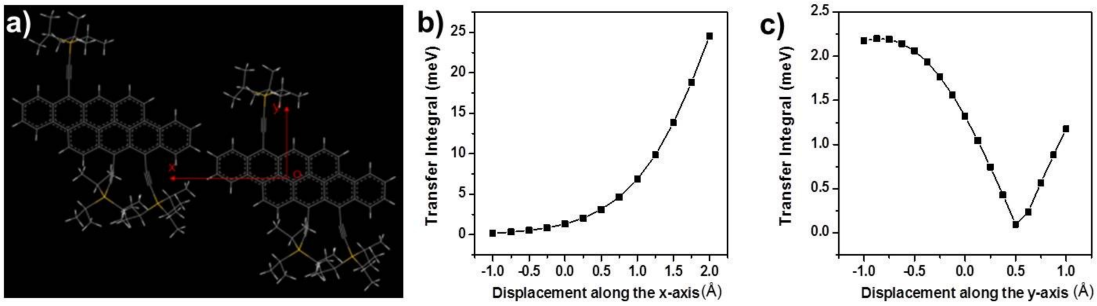

Figure S13. a) Illustration of the BT-3TIPS dimer along the b-direction of the crystal (the only possible charge-transport direction inferred from the crystal structure); b) the evolution of hole transfer integral as a function of the molecular displacements along x-axis and c) along y-axis.

Section 8. MALDI-TOF MS Spectral Profiles

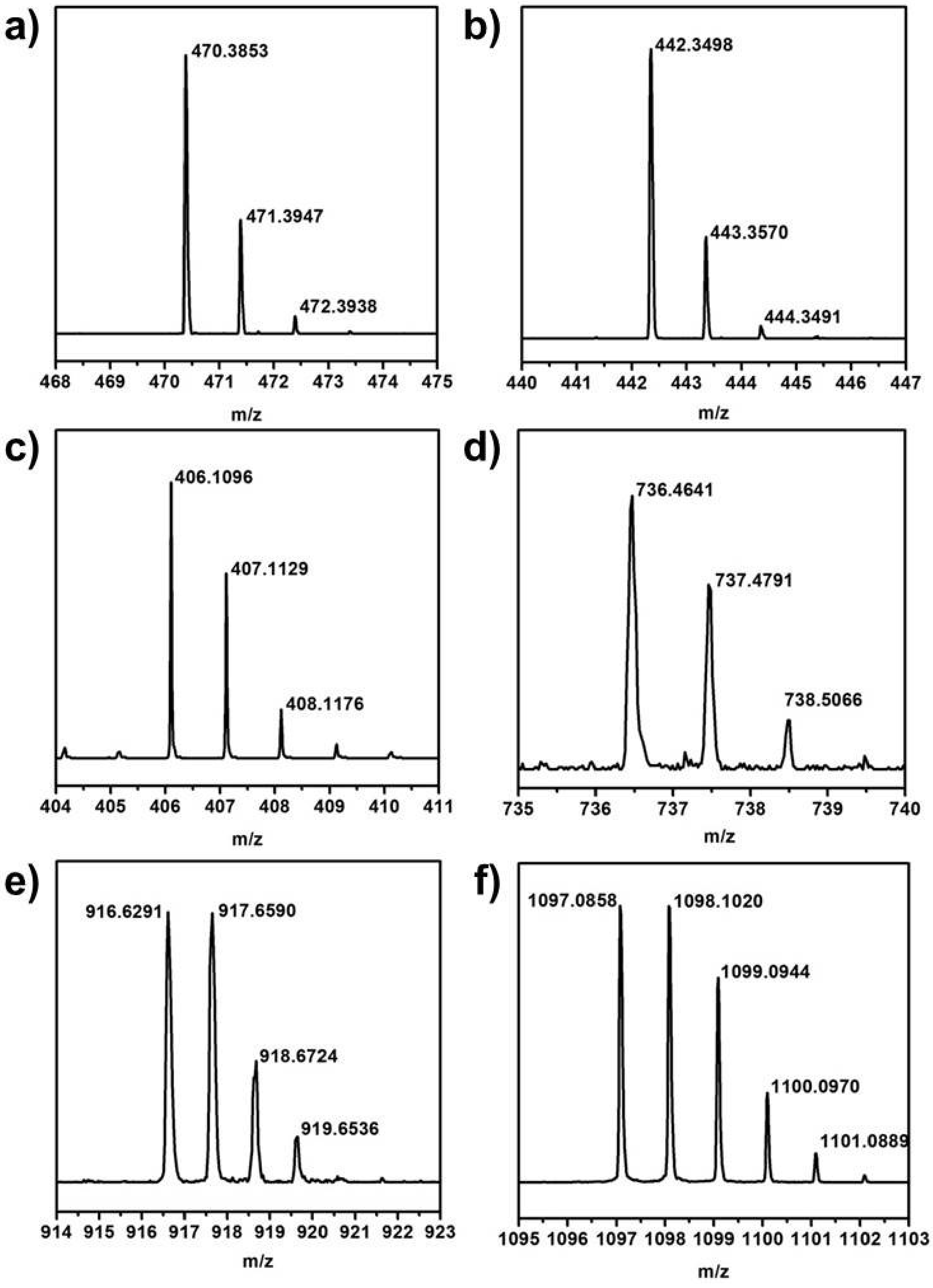

Figure S14. MALDI-TOF MS Spectral Profiles of a) **2,** b) **3**, c) **4**, d) **BT-2TIPS**, e) **BT-3TIPS**, f) **BT-4TIPS**.

Section 9. ^{1}H NMR & ^{13}C NMR Spectral Profiles

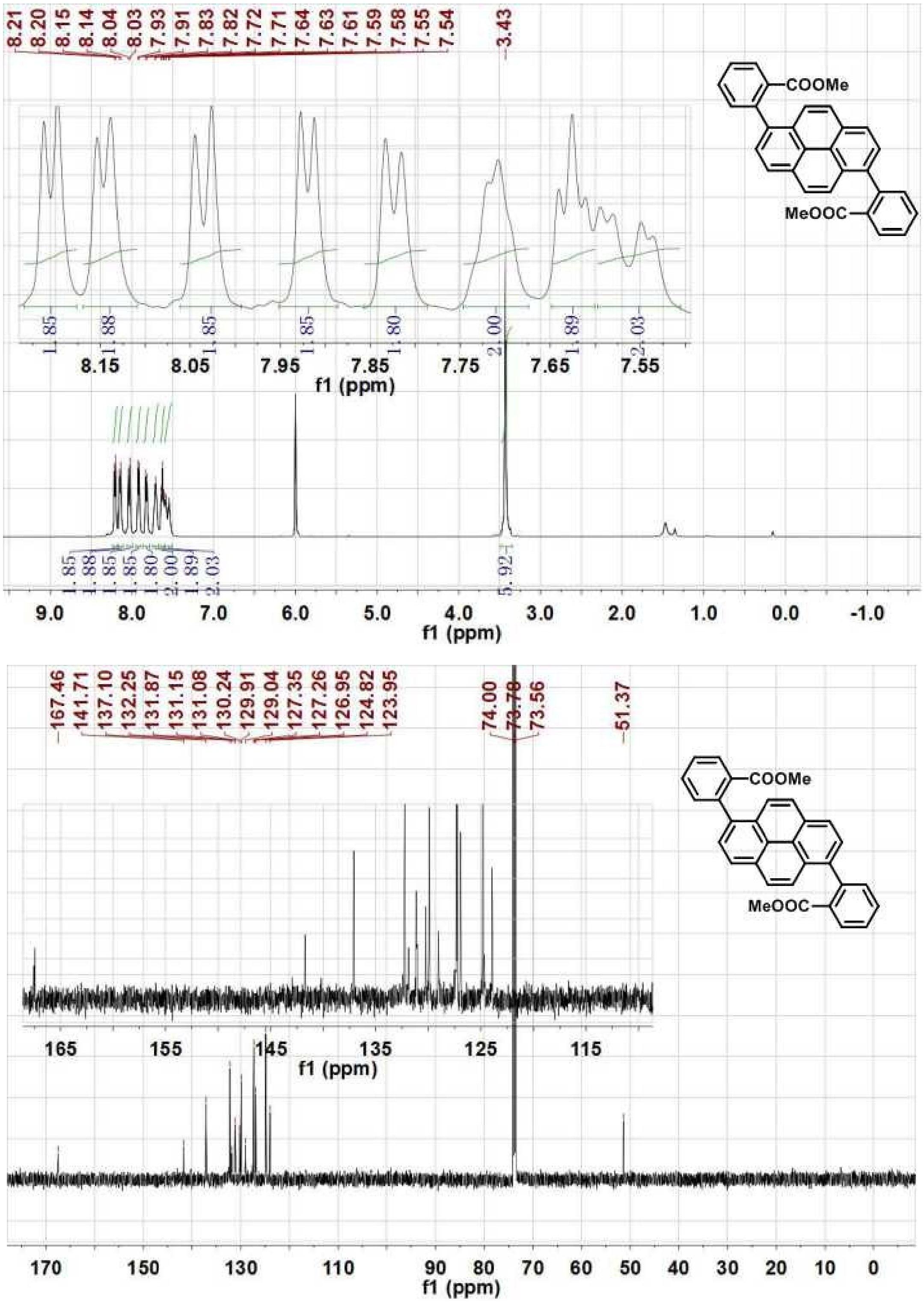

Figure S15. NMR spectra of compound **2** at 373 K ($C_2D_2Cl_4$): a) ^{1}H NMR, and b) ^{13}C NMR.

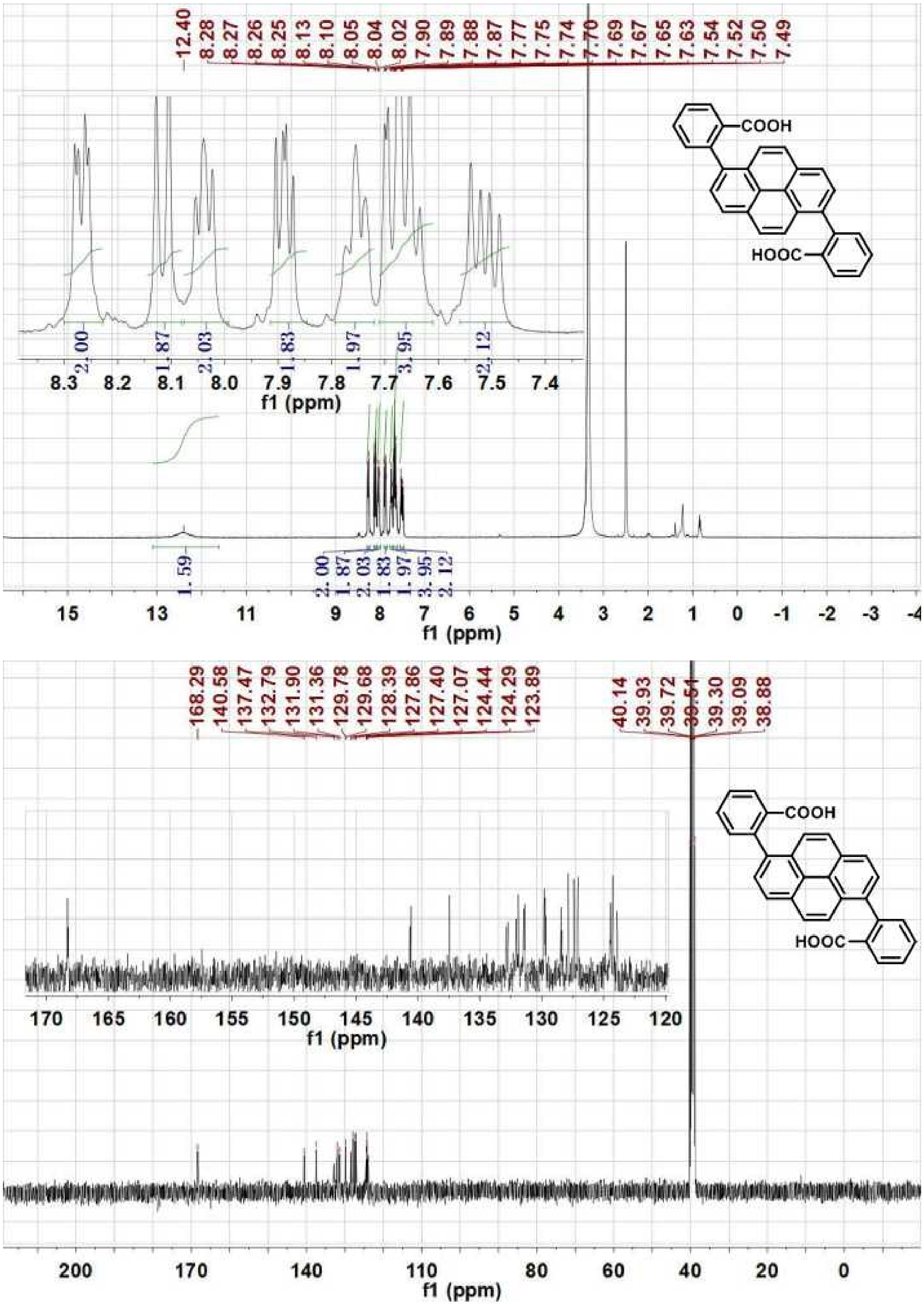

Figure S16. NMR spectra of compound **3** at room temperature (DMSO-d_6): a) ^{1}H NMR, and b) ^{13}C NMR.

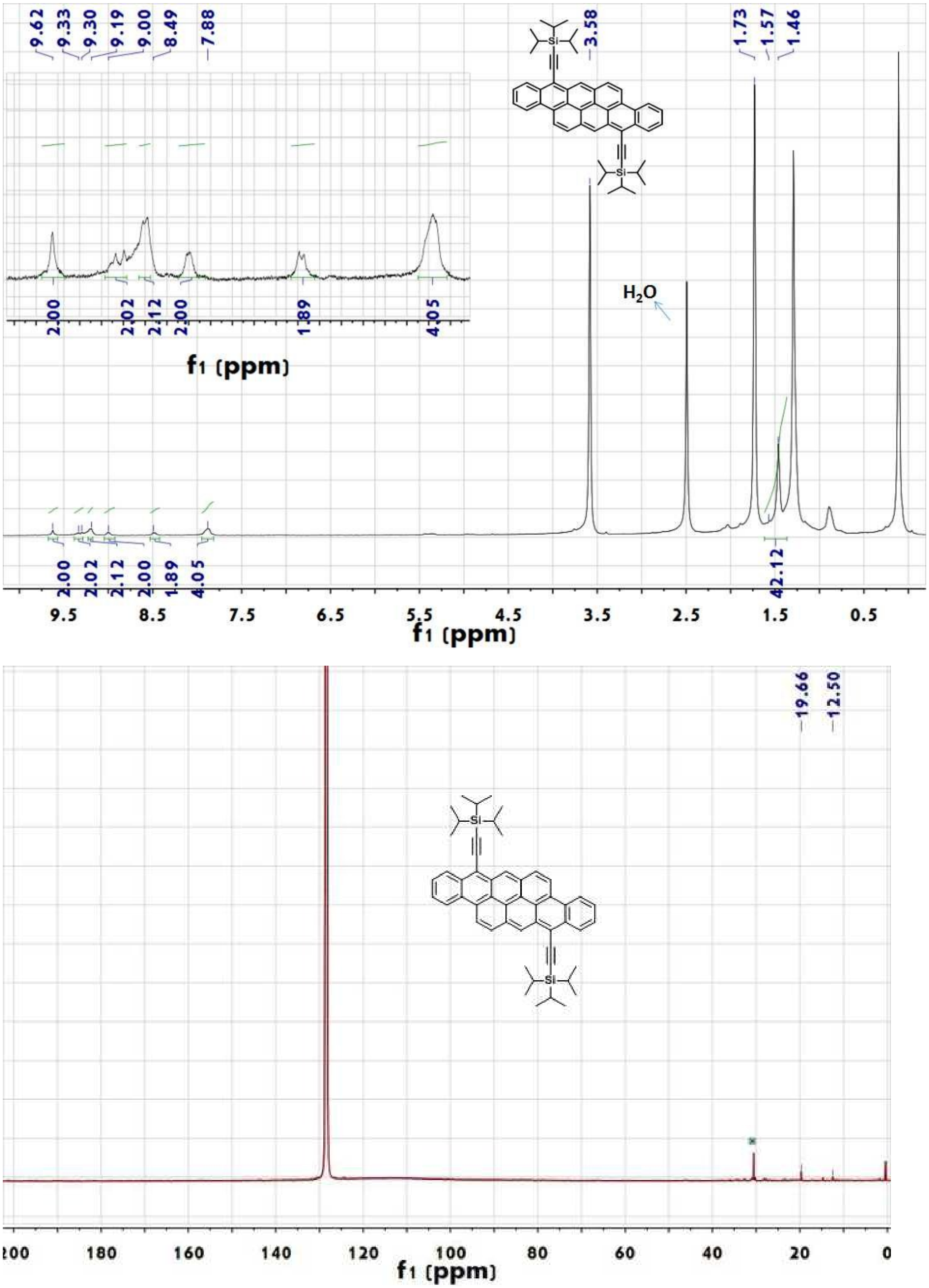

Figure S17. NMR spectra of compound BT-2TIPS at 273 K: a) ^{1}H NMR (400 MHz, d8-THF), and b) ^{13}C NMR (150 MHz, C_6D_6), x denotes grease.

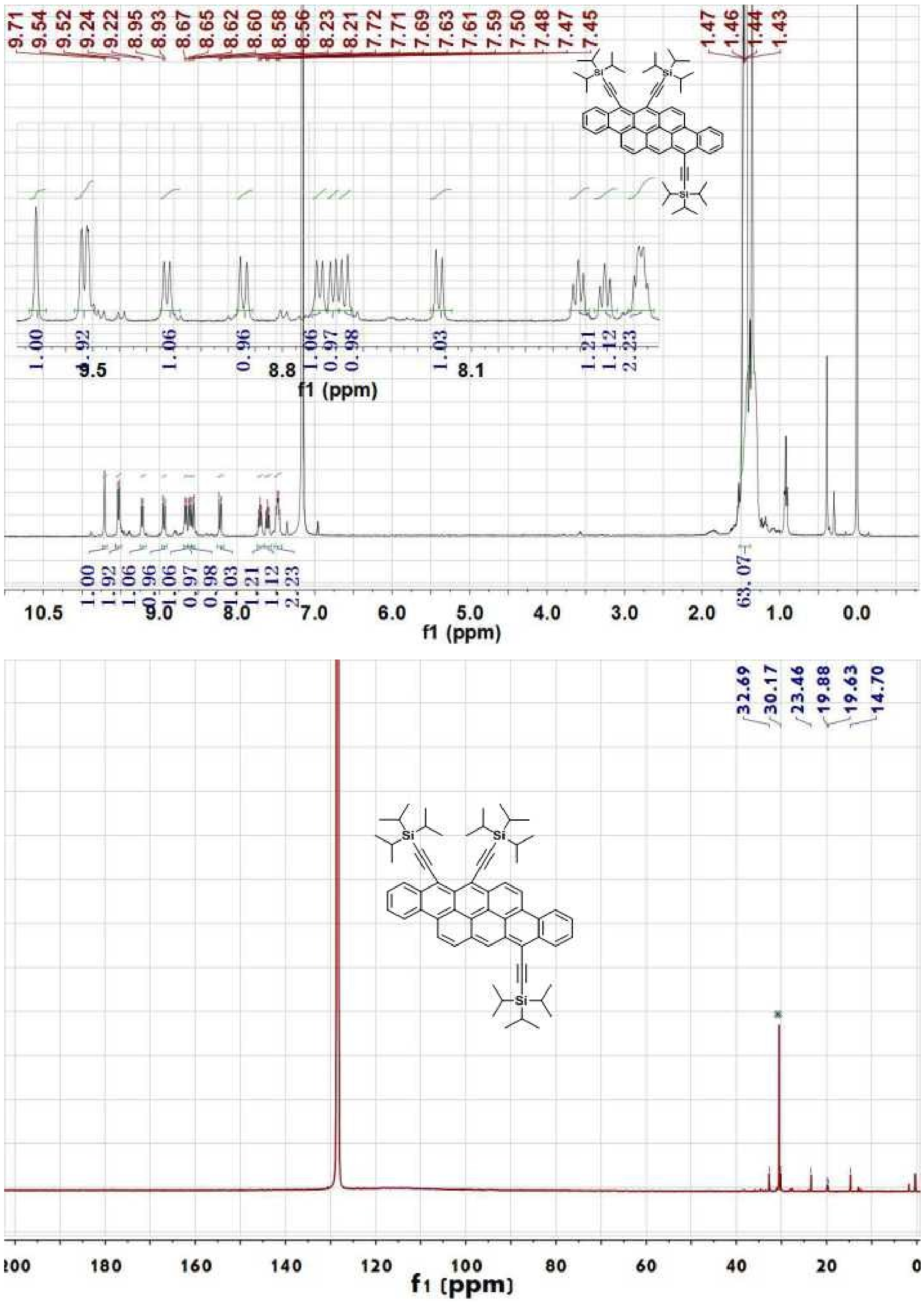

Figure S18. NMR spectra of compound BT-3TIPS at 273 K (C_6D_6): a) ^{1}H NMR, and b) ^{13}C NMR(150 MHz, C_6D_6), x denotes grease.

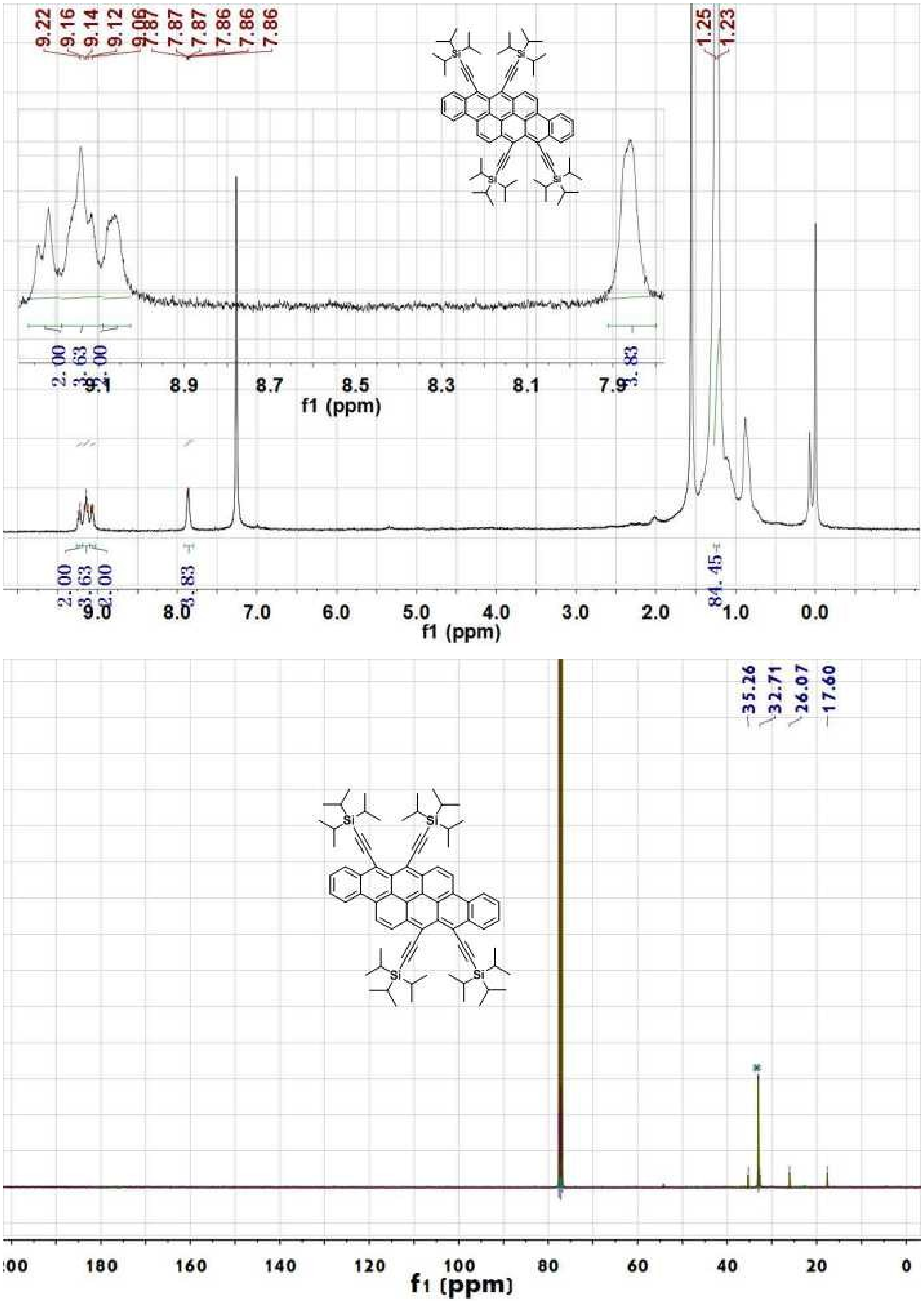

Figure S19. NMR spectra of compound BT-4TIPS at 273 K: a) ^{1}H NMR ($CDCl_3$), and b) ^{13}C NMR (100 MHz, $CDCl_3$), x denotes grease.

Section 10. Supporting Reference

[S1] Manna, B.; Chaudhari, A. K.; Joarder, B.; Karmakar, A.; Ghosh, S. K. *Angew. Chem. Int. Ed.* **2013**, *52*, 998-1002.

[S2] Wang, X. J.; Feng, L. H.; Zhang L. W. *Dyes and Pigments* **2013**, *97*, 318-323.

[S3] (a) Becke, A. D. *Phys.Rev. A,* **1988**, *38*, 3098-3100; (b) Lee, C.; Yang, W.; Parr, R. G., *Phys. Rev. B* **1988**, *37*, 785-789.

[S4] Frisch, M. J.; Trucks, G. W.; Schlegel, H. B.; Scuseria, G. E.; Robb, M. A.; Cheeseman, J. R.; Scalmani, G.; Barone, V.; Mennucci, B.; Petersson, G. A.; Nakatsuji, H.; Caricato, M.; Li, X.; Hratchian, H. P.; Izmaylov, A. F.; Bloino, J.; Zheng, G.; Sonnenberg, J. L.; Hada, M.; Ehara, M.; Toyota, K.; Fukuda, R.; Hasegawa, J.; Ishida, M.; Nakajima, T.; Honda, Y.; Kitao, O.; Nakai, H.; Vreven, T.; Montgomery Jr., J. A.; Peralta, J. E.; Ogliaro, F.; Bearpark, M. J.; Heyd, J.; Brothers, E. N.; Kudin, K. N.; Staroverov, V. N.; Kobayashi, R.; Normand, J.; Raghavachari, K.; Rendell, A. P.; Burant, J. C.; Iyengar, S. S.; Tomasi, J.; Cossi, M.; Rega, N.; Millam, N. J.; Klene, M.; Knox, J. E.; Cross, J. B.; Bakken, V.; Adamo, C.; Jaramillo, J.; Gomperts, R.; Stratmann, R. E.; Yazyev, O.; Austin, A. J.; Cammi, R.; Pomelli, C.; Ochterski, J. W.; Martin, R. L.; Morokuma, K.; Zakrzewski, V. G.; Voth, G. A.; Salvador, P.; Dannenberg, J. J.; Dapprich, S.; Daniels, A. D.; Farkas, Ö.; Foresman, J. B.; Ortiz, J. V.; Cioslowski, J.; Fox, D. J.; Gaussian, Inc.: Wallingford, CT, USA, 2009.

[S5] Senthilkumar, K.; Grozema, F. C.; Bickelhaupt, F. M.; Siebbeles, L. D. A., *J. Chem. Phys.*, **2003**, *119*, 9809.

[S6] Valeev, E. F.; Coropceanu, V.; da Silva Filho, D. A.; Salman, S.; Bredas, J. L. *J. Am. Chem. Soc.* **2006**, *128*, 9882.

[S7] L. Jiang, J. Gao, E. Wang, H. Li, Z. Wang, W. Hu and L. Jiang. *Adv. Mater.*, **2008**, ***20***, 2735-2740.

[S8] Q. Tang, Y. Tong, H. Li, Z. Ji, L. Li, W. Hu, Y. Liu and D. Zhu, *Adv. Mater.*, **2008**, *20*, 1511-1515.

[S9] R. A. Marcus, Electron transfer reactions in chemistry. Theory and experiment. Rev. Mod. Phys. 1993, 65, 599-610.

[S10] L. Wang, G. Nan, X. Yang, Q. Peng, Q. Li, Z. Shuai, *Chem. Soc. Rev.* **2010**, 39, 423-34.